A Simple Model of Fjord and Coastal Circulation Interaction[1]

JOHN M. KLINCK[2] AND JAMES J. O'BRIEN

Mesoscale Air–Sea Interaction Group, Florida State University, Tallahassee 32306

HARALD SVENDSEN

Geophysical Institute, University of Bergen, Bergen, Norway

(Manuscript received 5 September 1980, in final form 8 September 1981)

ABSTRACT

The dynamical interaction of a narrow fjord with a wind-driven coastal regime is investigated using a linear, two-layer numerical model. The Coriolis acceleration is important in the coastal regime but assumed to be unimportant in the fjord dynamics because $v = 0$. For a wide variety of wind conditions, bottom topography and model parameters, the wind-forced coastal circulation, with its geostrophic alongshore currents, has a strong effect on the circulation within the fjord.

These geostrophic currents control the free surface and pycnocline displacement at the fjord mouth, thereby strongly affecting fjord circulation. This mechanism is an alternative to the classical idea of hydraulic control at the mouth by sills or constrictions. Model simulations also show that the free surface slope is a baroclinic effect and that alongshore and across-shore winds affect the fjord differently. Alongshore winds produce flooding while up- and down-fjord winds simply set up the surface. We find that offshore winds can produce large velocity shear in the fjord which can have a significant effect on turbulent intensity and diffusion.

Data available from Norwegian fjords, the Strait of Juan de Fuca and Alberni Inlet, British Columbia, support this idea of dynamic control of fjord circulation by offshore wind-driven coastal currents.

1. Introduction

Since the Second World War, there has been increased interest in the study of deep-silled-fjord dynamics. One of the earliest of these studies (Saelen, 1946) indicated the importance of horizontal exchange between the fjord and coastal waters. He found that horizontal exchanges could account for differences between calculated and observed temperature distributions above sill level in Nordfjord. Similar arguments were put forward to explain hydrographic conditions in fjords on the western coast of North America (Pickard, 1961; Herlinveaux, 1962).

Recent investigations of fjords with deep sills on the western coast of Norway indicate that coastal waters act as an outer boundary to the intermediate layer [the layer below a thin (~2 m) surface freshwater layer] and that the mean circulation is shown to be closely connected with wind-induced fluctuations in the density field of adjacent coastal waters (Svendsen, 1980).

At one time, stratification of coastal water near fjords was thought to be controlled by seasonal runoff variations or by variations in the water properties of offshore currents. However, coastal upwelling studies of the 1960's and 1970's showed that the major changes in coastal stratification are wind induced (see Smith, 1968). This is confirmed by studies on the coast of Norway (Svendsen, 1971; Devold, 1972; Hermansen, 1974) which demonstrate that the major changes in coastal stratification are in response to winds.

Cannon (1971) found three distinct flow reversals in the Juan de Fuca submarine canyon which appeared to be related to coastal wind reversals. Svendsen and Utne (1973) suggest that renewal of deep water in Hardangerfjord is related to prolonged periods of upwelling-favorable coastal winds. A more detailed investigation of the Byfjord (Helle, 1975, 1978) clearly confirms this hypothesis.

In addition to coastal influences, processes within the fjord can produce circulation. Variations of vertical turbulent mass transport within a fjord cause pressure gradients which induce currents. This diffusively-driven circulation is usually quite weak and can be dominated by the stronger circulation due to coastal upwelling and downwelling. This overpowering of the diffusive circulation was evident in Josenfjord (Svendsen, 1977) where the mean flow

[1] Contribution 177 of the Geophysical Fluid Dynamics Institute, Florida State University.

[2] *Present affiliation:* Department of Oceanography, Texas A&M University, College Station 77843.

0022-3670/81/121612-15$07.75

in the upper part of the intermediate layer was opposite to the mean horizontal pressure field.

The above studies indicate considerable interaction between circulation patterns in fjords and on adjacent continental shelves. We investigate the nature of these interactions by constructing a model which simulates a narrow fjord connected to an adjacent coastal area.

The problem that we wish to investigate is inherently three-dimensional in space. Nevertheless, we can reduce the problem to two dimensions by assuming that the fjord is narrow (eliminating the Coriolis acceleration in the fjord). The resulting model, that of a layered channel, is well posed mathematically and can be solved efficiently.

This investigation required consideration of an ocean as well as a fjord. Several investigators have commented that it is sufficient to specify the free-surface and pycnocline elevation at the fjord mouth as a function of time to get the desired interaction. This suggestion leads to a mathematically ill-posed problem; once a wave (or characteristic) reflects from the end wall and returns, the elevations at the mouth cannot be specified independently and consistently.

The simplicity of this model is deliberate. We neglected non-linear and turbulent mixing effects in order to concentrate on fjord interactions with coastal circulation. The forcing in the fjord itself is also simple, only surface wind stress. At this point, we are not considering circulation forced by freshwater runoff within the fjord.

Several important results are obtained from this simple model. Most notable is that the offshore geostrophic circulation strongly controls hydrographic conditions and circulation within the fjord. Classical fjord circulation theory assumes that topographic effects at the mouth are the controlling factors (Strommel and Farmer, 1952; Long, 1975; Pearson and Winter, 1978; Stigebrandt, 1980, 1981). The present research shows an alternate control mechanism: offshore geostrophic circulation.

The model responds differently to alongshore and across-shore wind stress. If the model is forced by across-shore (up- and down-fjord) winds, there is an induced tilt in the free surface and pycnocline, but the total volume of water within the fjord remains constant. On the other hand, if the wind is strictly alongshore, a net transport into or out of the fjord produces flooding or emptying of the fjord as a whole.

Two final observations about fjord dynamics are made from the model results. The free-surface slope is a reflection of the pycnocline slope, i.e., it is baroclinic, not barotropic. The velocity shear is large in some cases which can have a strong effect on vertical diffusion.

The assumptions used to construct the model are discussed in Section 2. In addition, governing equations and boundary conditions are presented, together with the numerical solution techniques. Model results for a typical deep, narrow fjord forced by a constant wind stress are presented in Section 3. The effects of variable winds and sills are considered in Section 4. A simulation of the Strait of Juan de Fuca is also discussed. Section 5 contains conclusions of the research and points to possible extensions of the model.

2. Model formulation

The principal question investigated in this study is the nature of the dynamical interactions of a rotating, stratified, wind-driven coastal regime with a non-rotating, stratified narrow fjord. Our model is constructed by formulating the appropriate governing equations for the coast and fjord independently and matching the solutions at the junction point of the two regimes.

a. Fjord model

Typical fjord widths are in the 2–5 km range while a typical baroclinic Rossby radius of deformation ($\lambda = g'H^{1/2}f^{-1}$) is $\sim$10 km ($g' = 2$ cm s^{-2}, $H = 50$ m, $f = 10^{-4}$ s^{-1}). In addition, the narrowness of the fjord reduces the cross-fjord flow to zero, which removes the influence of the Coriolis acceleration. Therefore, rotational dynamics will have, at best, only secondary importance inside narrow fjords. In wide estuaries, this will not be true.

The influence of density stratification in a silled fjord is determined from a series of density measurements by Svendsen (1977) in Josenfjord on the west coast of Norway. A typical density profile (Fig. 1a) was used to calculate the squared buoyancy frequency (Fig. 1a) from which vertical modes were obtained. (For a discussion of vertical modes, see Pedlosky, 1979, p. 356 ff). The first five modal functions were calculated; the first and second are shown in Figs. 1b and 1c. The second eigenvalue (equivalent depth) is approximately half of the first and the rest of the eigenvalues decrease as n^{-2}, where n is the mode number. At present we are comparing current meter records from Josenfjord with the vertical modal functions to determine the number of layers which will best represent the fjord circulation. We have constructed a two-layer model as a first approximation. Later models can incorporate more layers if necessary. This analysis ignores a thin (<2 m thick) layer of brackish ($\sigma_t < 10$) water which appears in most fjords throughout the greater part of the year. The dynamical importance of this fresh layer is discussed later in light of some model results. Nonlinear and vertical mixing effects are excluded at this point to make the model as simple as

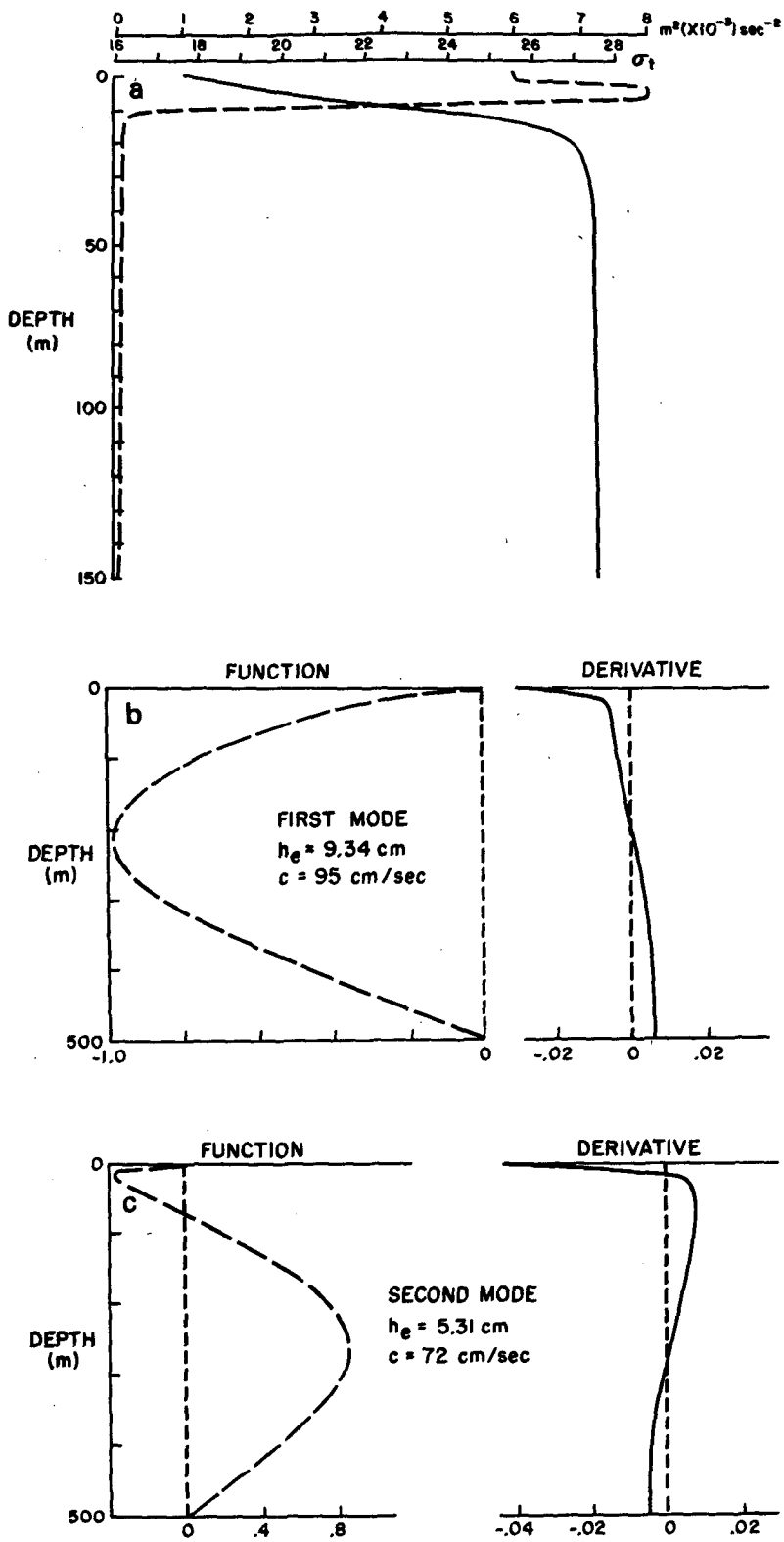

FIG. 1. (a) Typical density profile from a fjord. Surface (~2 m thick) freshwater layer is not included. The dashed line is the calculated buoyancy frequency squared. (b, c) First and second vertical internal modes. The dashed line is the structure of the vertical velocity and the solid line is the structure of the horizontal velocity. Equivalent depth and phase speed are indicated.

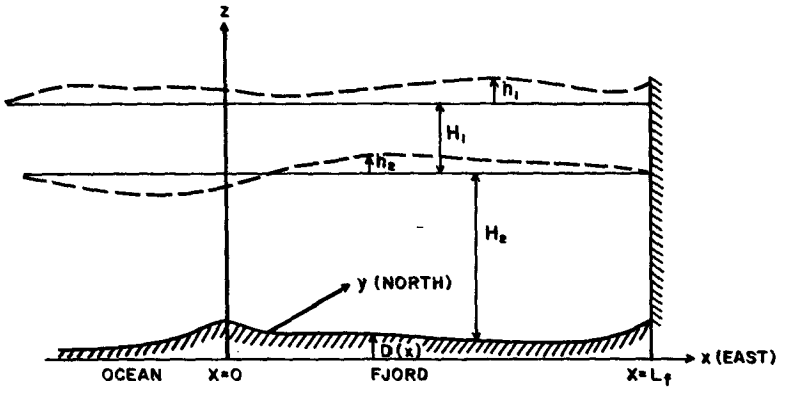

FIG. 2. Model geometry and variables. The β-plane ocean is joined to a non-rotating fjord at $x = 0$. The ocean basin is 1000 km wide to avoid direct influence of the western boundary.

possible. Shear stress is applied at the surface, but no vertical frictional effects are included at the interface or bottom. A small amount of horizontal friction is included ($A = 10^5$ cm^2 s^{-1}).

b. *Shelf model*

The coastal upwelling dynamics of Hurlburt and Thompson (1973) are used to model the coastal area. Their results indicate that an alongshore pressure gradient is crucial in the dynamics of coastal upwelling. In a vertical-plane model, this pressure gradient is retained implicitly by formulating a vorticity equation and allowing f to vary, i.e., the coastal dynamics are on a β-plane.

As in the fjord, nonlinear and mixing processes are ignored. Except for surface stress, vertical friction is not included. Also, a small horizontal friction effect is included, mainly to bring alongshore velocities to zero at the coast.

c. *Model equations*

The equations of motion for transport in the oceanic part of the two-layer model, consistent with the above considerations are

$$u_{1t} = fv_1 - gH_1(h_1 + h_2 + D)_x + \tau^x + Au_{1xx}, \quad (1)$$

$$v_{1xt} = -\beta v_1 - fu_{1x} + \tau_x{}^y + Av_{1xxx}, \quad (2)$$

$$h_{1t} = -u_{1x}, \quad (3)$$

$$u_{2t} = fv_2 - gH_2(h_1 + h_2 + D)_x + g'H_2h_{1x} + Au_{2xx}, \quad (4)$$

$$v_{2xt} = -\beta v_2 - fu_{2x} + Av_{2xxx}, \quad (5)$$

$$h_{2t} = -u_{2x}, \quad (6)$$

where subscripts indicate partial derivatives. The notation is standard and is explained in the Appendix. Note, however, that u and v denote vertically integrated transports.

The model geometry is illustrated in Fig. 2. The point $x = 0$ is the junction between the shelf and the fjord, with the shelf occupying the interval $[-L_o, 0]$ and the fjord occupying $[0, L_f]$. L_f and L_o are the lengths of the fjord and ocean, respectively.

The governing equations for the fjord are (1) and (4) with $f = 0$, and (3) and (6). Eqs. (2) and (5) do not apply because there is no v transport in the fjord.

d. *Further model considerations*

Eqs. (1)–(6) appear to match an infinitely long coastal regime with a thin fjord channel. Such a situation would require the across-shore transport in the ocean to vanish for the transport in the fjord to be finite. An alternate interpretation given below avoids this problem.

Consider a channel of constant width stretching from $x = -L_o$ to $x = L_f$. Let the end walls be fixed and impermeable. The sidewalls of the channel from $x = 0$ to $x = L_f$ (the fjord part of the channel) are impermeable. On the other hand, the sidewalls in the ocean ($x = -L_o$ to $x = 0$) are totally permeable to water flow.

The dynamical equations for this situation are obtained by integrating the equations of motion over the two layers and across the width of the channel.

Integration of the v_y term in the continuity equation leaves equations of the form (3) or (6) with two additional terms: the difference of the v transport at either side wall. Within the fjord, these terms vanish because of the impermeable walls. In the oceanic region, where the walls are permeable, the extra terms do not vanish. However, if the channel width is less than the natural alongshore length scales, the variation of v across the channel is small and the terms cancel approximately. The shortest natural length scale of interest is the internal Rossby radius, which is of order 10 km. Therefore, if the channel is much narrower than the internal Rossby radius (which is assumed to be true in these simulations),

TABLE 1. Choice of parameters for a typical deep sill fjord.

$\Delta x = 2$ km	$H_1 = 20$ m
$\Delta t = 1$ h	$H_2 = 480$ m
$f = 10^{-4}$ s^{-1}	$L_f = 30$ km
$\beta = 10^{-13}$ cm^{-1} s^{-1}	$L_o = 970$ km
$g' = 4.5$ cm s^{-2}	$A = 10^5$ cm^2 s^{-1}

the continuity equations in the oceanic regime also have the form given by (3) and (6).

The y derivatives in the momentum equations also vanish using similar arguments. The alongshore pressure gradient term remains implicitly in the vorticity equation.

Therefore, Eqs. (1)–(6) are interpreted as a y average of the dynamical equations in a "leaky" channel. This problem is well posed mathematically without a mismatch of alongshore scales.

e. Matching and boundary conditions

The matching conditions between the two regions are continuity of transport and layer thickness.

The boundary conditions are

$$\left.\begin{aligned} u_i(x = -L_o) = v_i(x = -L_o) = 0, \\ v_i(x = 0) = 0, \\ u_i(x = L_f) = 0. \end{aligned}\right\} \quad (7)$$

for $i = 1, 2$.

One further boundary condition must be applied to the vorticity equation. We choose to apply the condition at the western oceanic boundary; conditions there are known better than at the eastern boundary. Because the oceanic regime obeys β-plane dynamics, a Munk-type western boundary current is available to balance the v transport due to wind stress curl in the interior.

The transport of the western boundary current is determined by the horizontal gradient of vorticity (v_{xx}) at the western wall ($x = -L_o$). For an expanded discussion of this condition, see Hurlburt and Thompson (1973). Rather than adjust the western boundary current to equal the Sverdrup transport exactly, the following approximation is used. The steady Munk boundary layer solution is obtained from $A\hat{v}_{xxx} - \beta\hat{v} = 0$ with the conditions that $\hat{v}(x = -L_o) = 0$ and $\hat{v}(x \to \infty) \to 0$. The solution is

$$\hat{v} = C \exp[-K(x + L_o)] \sin[\sqrt{3}K(x + L_o)], \quad (8)$$

where $K = 0.5\,\beta^{1/3} A^{-1/3}$ and C is a constant. The value of $\hat{v}_{xx}(x = -L_o)$ and $\int_{-L_o}^{\infty} \hat{v}dx$ are obtained in terms of C from (8).

The last condition on the two-layer model is that the interior transport across the plane of the model is balanced by the western boundary transport or

$$\int_{-L_o+\Delta}^{0} (v_1 + v_2)dx = -\int_{-L_o}^{\infty} \hat{v}dx,$$

where Δ is the thickness of the boundary layer. This relation determines C which is used to find $v_{xx}(x = -L_o)$.

The final boundary condition in each layer is

$$v_{i_{xx}}(x = -L_o) = H_i(H_1 + H_2)^{-1}\hat{v}_{xx}(x = -L_o) \quad (9)$$

for $i = 1, 2$. The constant in (9) divides the transport between the two layers.

f. Numerical procedure

The system of equations (1)–(6) with boundary conditions (7) and (9) is solved numerically using a staggered grid, centered-in-time finite-difference scheme; u_i, h_i are known at the same time on alternating x nodes, while v_i is known at the same nodes as u_i at intermediate times.

In the x-momentum equations, (1) and (4), the acceleration term uses a trapezoidal time integration, the pressure gradient and viscosity terms are averaged over old and new time steps, and the Coriolis term is evaluated explicitly. This setup is similar to the semi-implicit scheme discussed by O'Brien and Hurlburt (1972).

The continuity equations (3) and (6) are also treated implicitly with the divergence term averaged over new and old time steps.

In the vorticity equations, (2) and (5), forward differences are used for both x and t, and the β term is averaged over both time and space. The viscous term is evaluated by the appropriate central difference in x at the old time step. This approximation for the viscous term allows explicit calculation of the v transports at each time step. The alternative to this approximation requires the solution of a system of forced, linear algebraic equations with a quadridiagonal coefficient matrix, which greatly increases the required calculations at each time step.

The time-differenced equations reduce to two coupled, forced, ordinary differential equations in x for the u transport at the new time. The two equations can be uncoupled by forming new variables

$$q_j = (u_1 + \lambda_j u_2), \quad j = 1, 2.$$

For a suitable choice of λ_j, the equations uncouple into two equations of the form

$$q_j - \alpha_j q_{jxx} = F_j, \quad j = 1, 2, \quad (10)$$

where α_j is a constant and F_j is the known forcing function composed of variables from the old time step. Note that because the Coriolis term is explicit, its effect is contained solely in the forcing function F_j and that the x momentum equations for the fjord

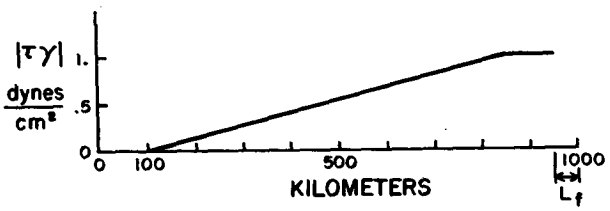

FIG. 3. Structure of the meridional wind across the ocean basin. Upwelling or downwelling at the eastern boundary is determined by the sign of τ^y.

also reduce to (10) with a slightly modified forcing function.

Using a central-difference form for the second derivative in (10) reduces the differential equations to a set of forced, linear algebraic equations with a tridiagonal coefficient matrix. Fast, direct methods exist for solving such systems of equations (e.g., Issacson and Keller, 1966, p. 55 ff).

3. Basic case

The simplicity of the model allows us to test large areas of the parameter space. However, to maintain some order in investigating various dynamical situations, the parameters are chosen to correspond to fjords for which appropriate data are available. The basic case is typical of fjords on the southwestern

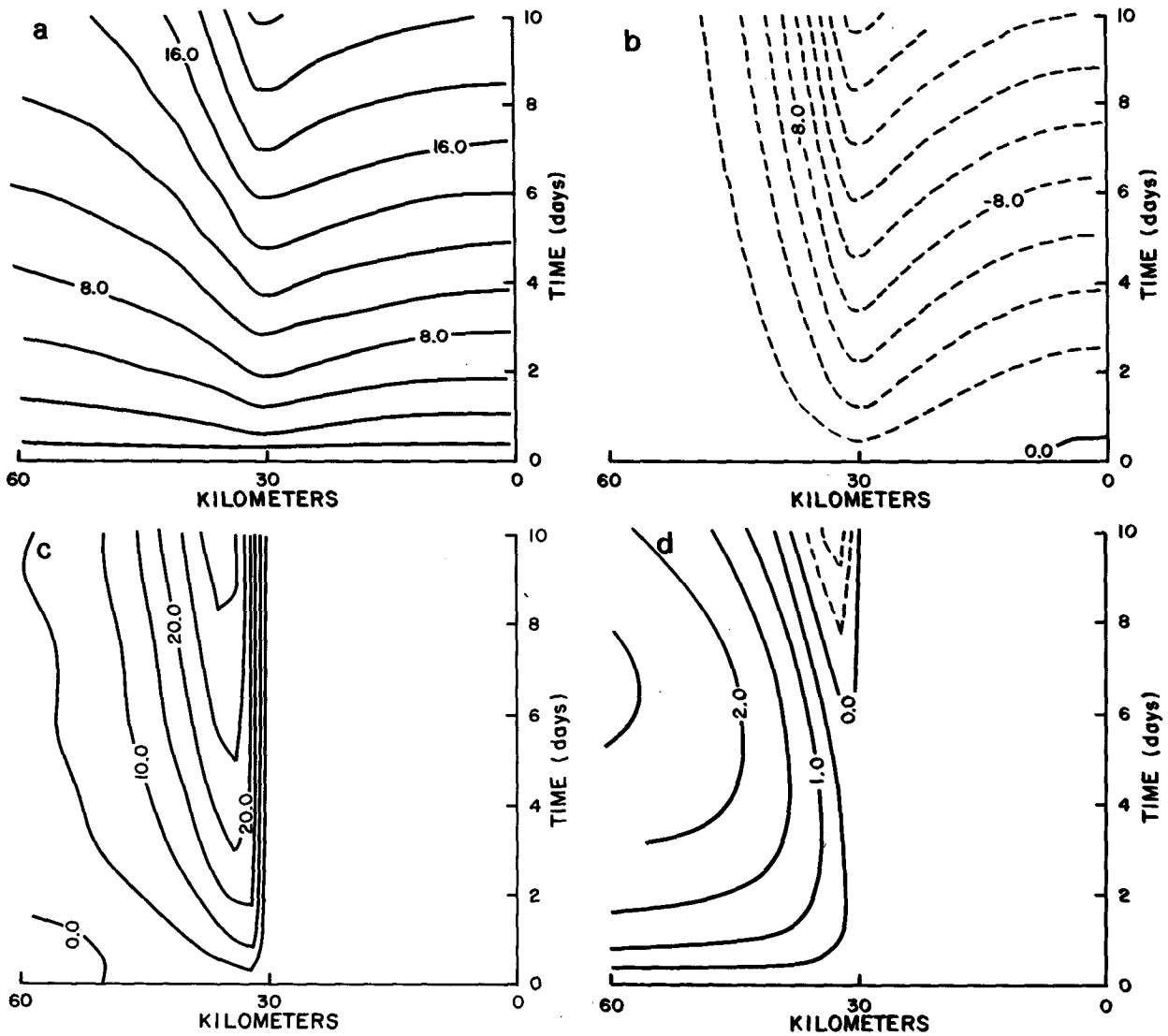

FIG. 4. Typical fjord simulation. Total depth is 500 m with no bottom topography. Other parameters are given in Table 1. τ^y is northward at the eastern boundary, impulsively started at $t = 0$. (a) Free surface, (b) pycnocline and (c, d) alongshore velocity in each layer contoured in x–t plane. Dashed lines indicate negative values. Contour intervals are (a) 2 cm, (b) 2 m, (c) 5 cm s^{-1}, (d) 0.5 cm s^{-1}. Distance is measured from the fjord wall.

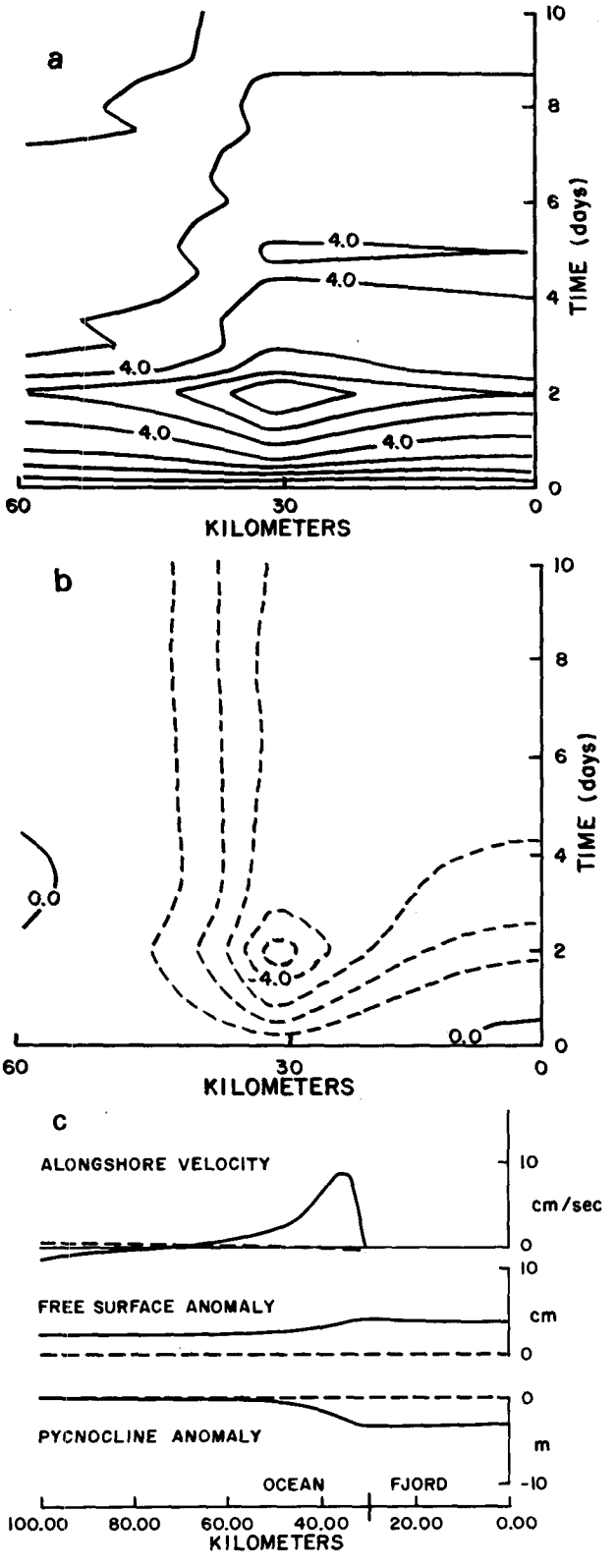

FIG. 5. Basic case forced for 48 h. (a) Free surface and (b) pycnocline anomaly are contoured in x and time. Dashed lines show negative anomalies. (c) Alongshore velocity, free surface and pycnocline as a function of position after five days. The dashed alongshore velocity is the lower layer; the solid line is for the upper layer. Contour intervals are (a) 1 cm, (b) 1 m.

coast of Norway. The parameters are listed in Table 1.

The model, started from rest, is forced by wind stress curl over the main ocean basin. The structure of the assumed wind field is shown in Fig. 3. The sign of the wind at the eastern boundary determines if there is upwelling or downwelling at the mouth of the fjord.

The model results for downwelling conditions are shown in Fig. 4. Ekman pumping causes the free surface to rise, with the largest elevation occurring at the junction point. At the same time, the pycnocline deepens, driving an outward transport in the lower layer of the fjord. Within one day of the start of the wind, the pycnocline is such that the lower layer pressure gradient is nearly zero. As long as the wind blows, this small lower layer flow balances the incoming, upper layer Ekman flux.

A northward coastal jet which is in geostrophic balance with the surface pressure gradient forms on the oceanic side of the junction point. After a longer time (10 days), a southward oceanic undercurrent also forms. This geostrophic, alongshore current system, with its surface and pycnocline displacements, controls the thickness of the two layers at the fjord–shelf junction and thereby controls the circulation in the fjord.

This offshore control is seen explicitly if the basic case is forced by the wind for 48 h, after which the wind is turned off. An x–t contour plot (Figs. 5a and 5b) of the free surface and pycnocline anomaly show clearly that the slopes inside the fjord vanish a day and a half after cessation of the wind, but offshore, the slopes of the free surface and pycnocline remain. These offshore slopes prevent the layer thicknesses inside the fjord from returning to their initial values. Fig. 5c shows why the flow does not relax. The geostrophic coastal currents maintain the offshore surface and pycnocline slopes, even in the absence of the wind.

Two additional features of this simulation need to be emphasized. First of all, notice in Fig. 4a that the free surface in the fjord continues to rise with time. After ten days of constant winds, water at the head has risen 20 cm from its initial level and the pycnocline is depressed 14 m. This flooding is the result of Ekman transport from the alongshore wind pushing water into the fjord. Such dynamics are not available within the fjord, so the water "piles up" at the junction point until the pressure gradient can transport the water into the fjord.

The second notable result is that the free surface slope is a baroclinic effect. If the flow were barotropic, there would be a tilt of the free surface but not

of the pycnocline. Fig. 4b shows that the fjord flow is baroclinic to some extent. For a purely baroclinic flow, the surface and pycnocline slopes are proportional with $\Delta\rho/\rho$ as the proportionality constant. A short calculation shows that the fjord circulation is almost entirely baroclinic. The pycnocline slope at some time is obtained from Fig. 4b [e.g., day six when the slope is 4.5 m(30 km)$^{-1}$]. The density difference is 4.5×10^{-3}. Therefore, for the flow to be purely baroclinic, the free surface slope must be 2 cm(30 km)$^{-1}$. Fig. 4a shows that this is the model result. Thus, the free-surface slope is essentially a reflection of the pycnocline displacement, i.e., it is baroclinic.

The basic case results were calculated for a southward coastal wind stress which gives upwelling at the coast. The model dynamics are the same for either direction of the wind, only the response is reversed. However, the surface layer becomes thinner with time causing very large velocities due to a venturi effect. The pycnocline eventually reaches the free surface and the model breaks down.

The results of this simple calculation are supported by wind and current measurements from a fjord system on the southwestern coast of Norway (Fig. 6). Winds were measured off the coast on Utsira Island (W2) and in Josenfjord (W1) and Hylsfjord (W3). Current meter records from Station B in Josenfjord indicate the flow patterns. Sea level slope is obtained from tide gages at Stavanger and Sand. All of these measurements are smoothed with a 24 h sliding mean.

The close correlation of the surface (1.5 m) fjord currents (Fig. 7b) with the up- and down-fjord winds (Fig. 7a) is evident. There are times, however, when the surface flow is opposite to the surface wind stress, such as 12, 20, 26 and 27 June. These times correspond to periods of strong, southward coastal wind stress (Fig. 7c). Such southward stress gives offshore Ekman transport of the surface water, thereby pulling water out of the fjord. Support for this calculation is provided by current records at 1.5, 5 and 10 m (Figs. 7b, 7d, 7e) which show down-fjord currents. There is a small compensating up-fjord flow in the lower layers during these wind events.

The model response to southward wind is obtained from Fig. 4 by changing the sign of the results (because of model linearity). The response is then a falling of the free surface and a rising of the pycnocline. The free surface slopes downward from the head to the mouth of the fjord while the pycnocline slopes downward from the mouth to the head. These pressure gradients drive outward flow in the upper layer of the fjord and inward flow in the lower layer. This flow pattern is in agreement with the current meter records in Fig. 7. Note that during each of the three events, the circulation in the fjord is opposite to that expected from the direction of the wind in the fjord.

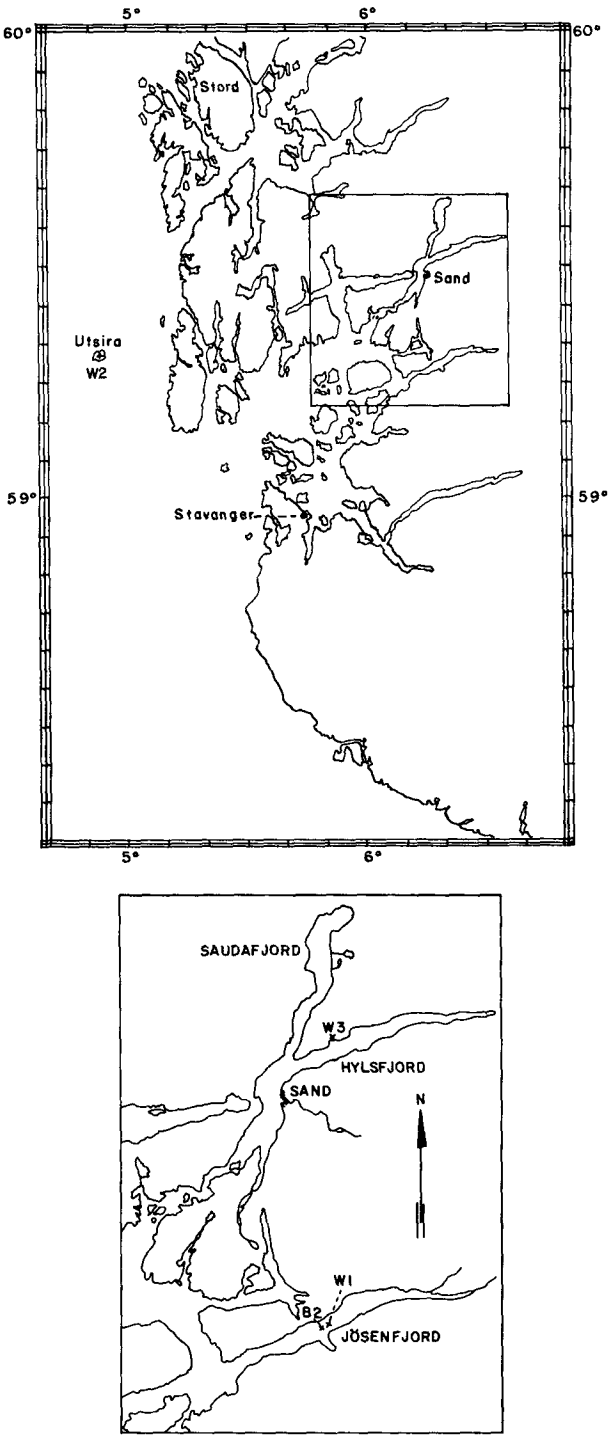

FIG. 6. Southwestern coast of Norway. The inset locates various fjord stations discussed in the text.

Further evidence of this offshore control of the fjord circulation is shown in Fig. 8. The mean up- and down-fjord current is shown to be strongly af-

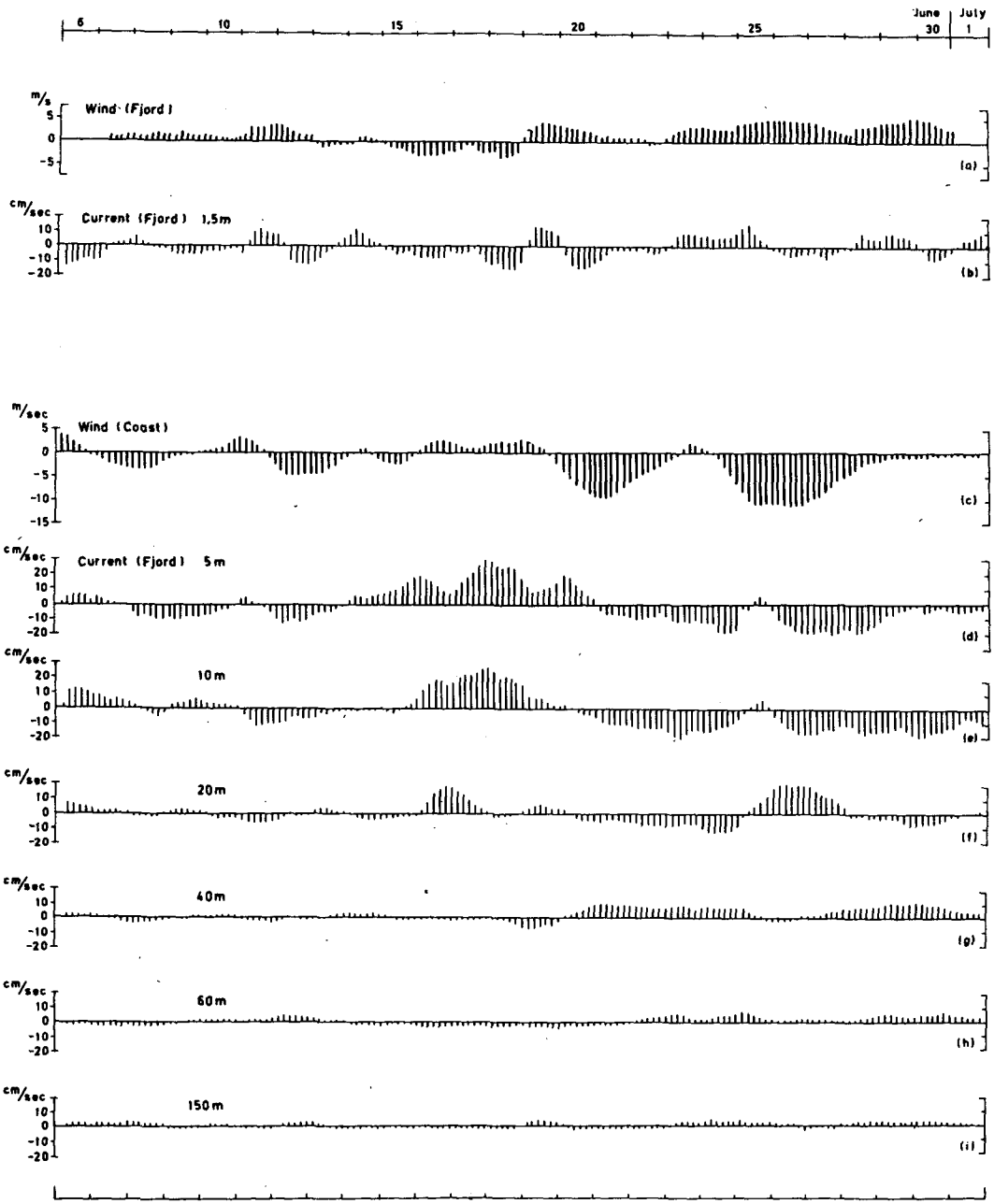

FIG. 7. Fjord and coastal winds with current measurements at Station B. Up- and down-fjord winds were measured at Station W1 (Josenfjord) while alongshore coastal winds were measured at W2 (Utsira). The wind and current records are smoothed with a 24 h sliding mean.

fected by the coastal winds. Observe, especially, 18 and 27 June.

Sea level slope (Fig. 9) provides some support for the model results, although not as clear-cut as the previous current data. The calculated difference of water level at the two stations indicates a net downward slope of the free surface from the head to the mouth. Nevertheless, there is some indication of increasing (decreasing) coastal free surface elevation with northward (southward) coastal wind stress.

4. Additional remarks

a. Sills

Sills are present in most fjords; hence, their effect on the circulation must be considered. We ran the basic case with a parabolic sill 400 m high and 20 km

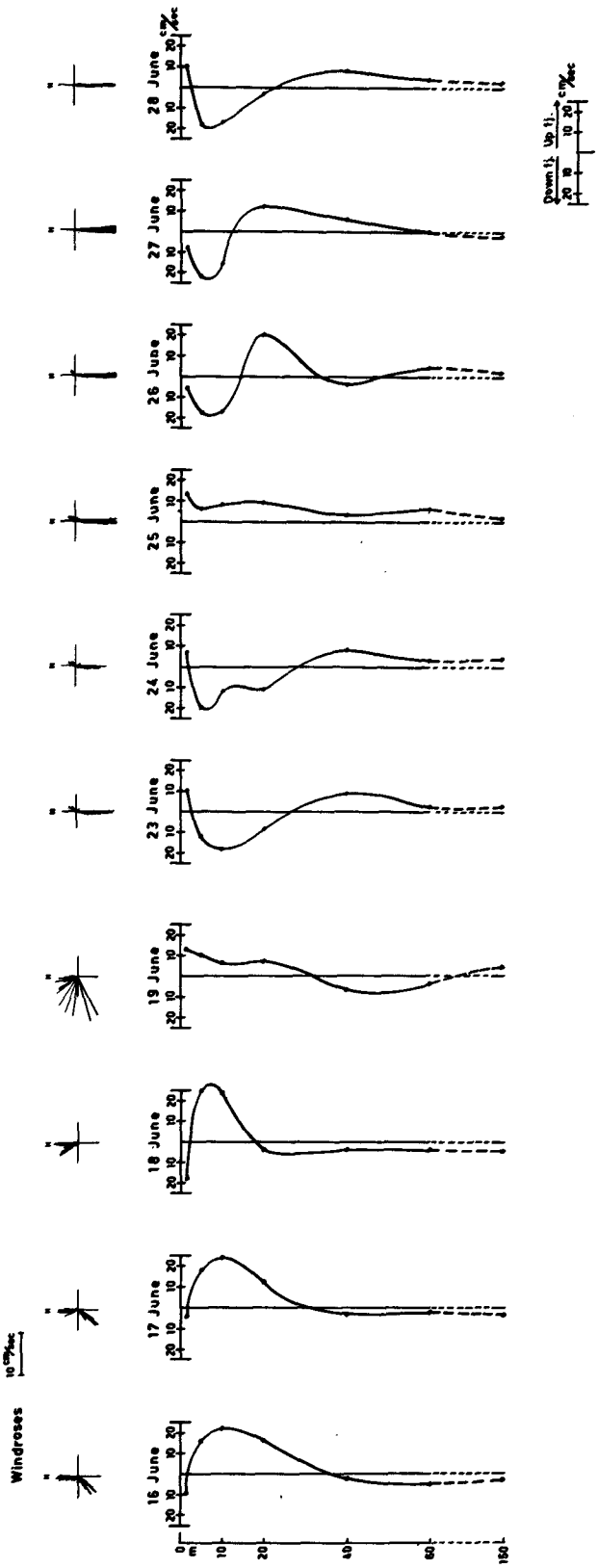

FIG. 8. Mean current profiles from Station B with wind roses from station W2 on the coast. Currents are 24 h means evaluated at noon on the day indicated. The wind roses are six-hourly coastal wind measurements for the day indicated and the previous two days.

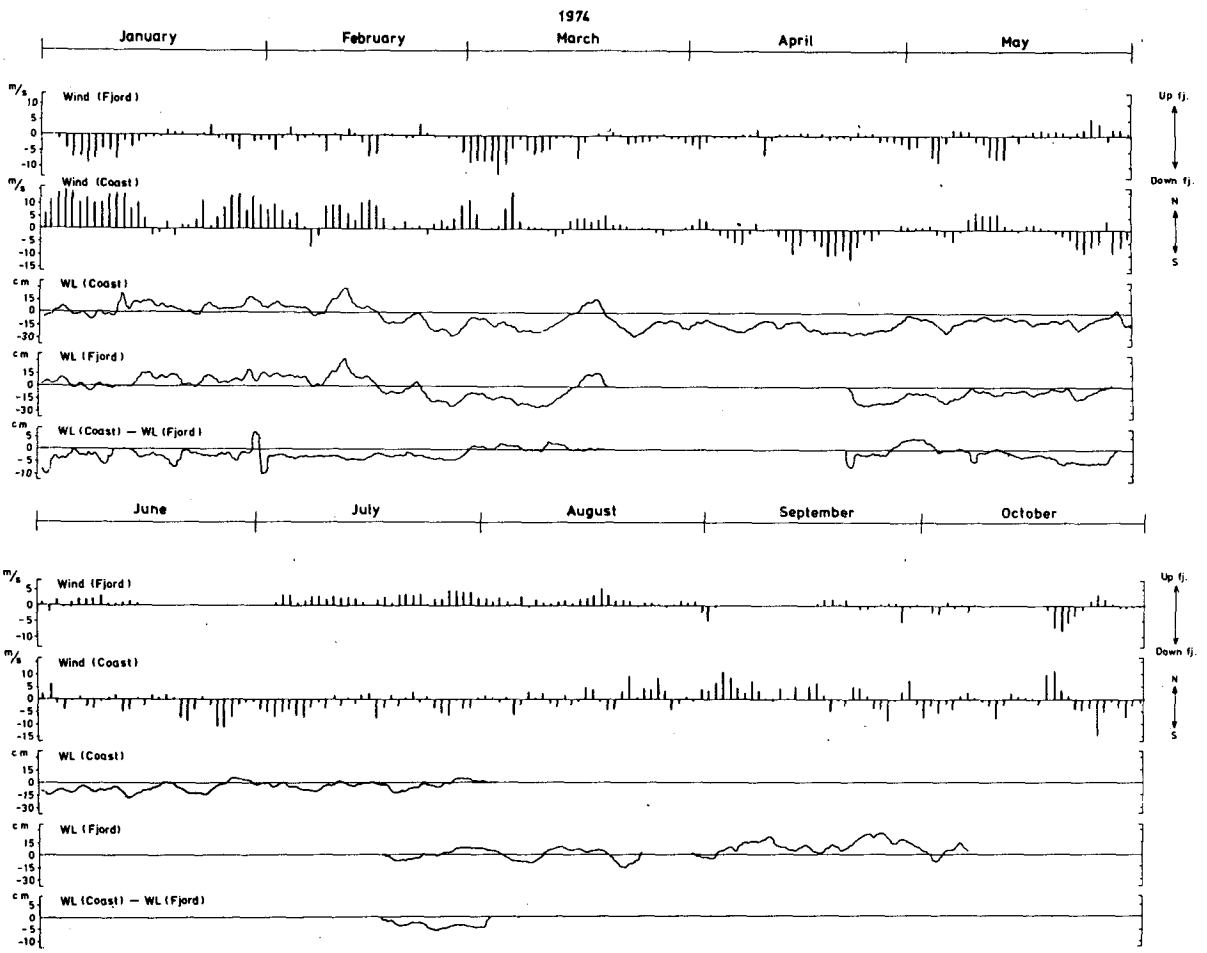

FIG. 9. Coastal and fjord sea level and winds. Fjord winds are measured at W3 in Hylsfjord and the coastal winds are from W2. Stavanger and Sand are the coastal and fjord sea level stations, respectively. WL curves are 24 h sliding means of the water level records. The fifth plot in each set is the difference in water level between the coastal and fjord stations.

wide, centered at the junction point. Even though this sill takes up 80% of the total depth, its dynamical effect on the transport in either layer is indiscernible. The velocities were much larger in the vicinity of the sill but this is caused by thinning of the layers, a venturi effect. Several other cases with sills were calculated; none showed any major effect due to the sill.

b. *Five-day periodic winds*

Rarely do winds persist for many days, so the effect of time-varying wind forcing must be considered. As a first approximation, the winds are given a sinusoidal temporal variation with a 5-day period. This choice approximates the synoptic variation of the winds.

The response is indicated in $x-t$ contour plots (Fig. 10). As before, the largest anomaly in the free surface and interface occurs at the junction of the two regimes. The asymmetry of the response as the wind reverses is due to the time required to reverse the circulation pattern. During the first 2.5 days, the circulation spins up from rest. During the second 2.5 days, the wind blows against the prevailing circulation which must be stopped before being reversed. The response is always smaller during the second half period than during the first. Circulation near the fjord has a short enough response time that it keeps up with variations in the wind.

c. *Sea breeze*

The effects of sea breeze forcing on the model also is considered. The up- and down-fjord wind is purely sinusoidal with a 24 h period and an amplitude of 0.4 dyn cm^{-2}. It is applied from the head of the fjord to 20 km offshore of the junction point. There is no alongshore wind.

This simulation (Fig. 11) again shows the strong control that the geostrophic coastal currents have over the fjord circulation. After two days, the major

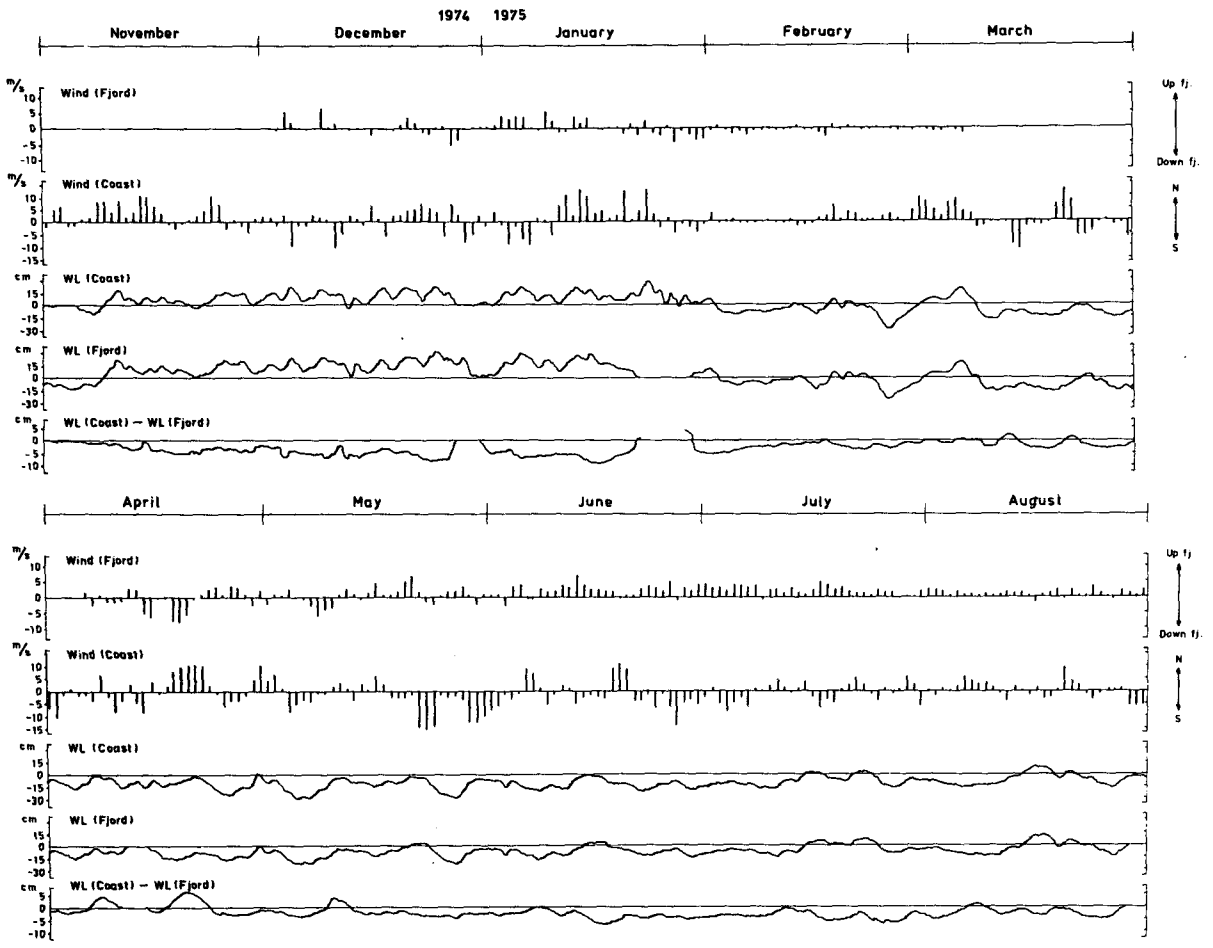

FIG. 9. (*Continued*)

surface and internal slopes are set up and are balanced by the coastal currents. The major sea breeze effect in the fjord is within 2 km of the head. Here the layer thicknesses oscillate slightly with a 24 h period. A similar small oscillation is found on the seaward side of the strong coastal current.

The fjord responds differently to up- and down-fjord winds than it does to alongshore coastal winds. The free surface is set up such that there is no net change in the volume of water in the fjord. The Ekman transport for across-shore winds is along the coast, so there is no transport to fill or empty the fjord. Note also that the free surface is baroclinic as it was for alongshore wind forcing.

The largest onshore–offshore currents in the upper and lower layers are 3 and 0.1 cm s^{-1}, respectively. The surface current reverses in phase with the wind, while the lower layer current is out of phase with the wind.

This model result is contrary to the findings of Svendsen and Thompson (1978, Fig. 10). Their averages for the diurnal variation in Josenfjord show that only the surface (1.5 m) current responds directly to the wind. At 5 and 10 m, the current is out of phase with the wind and from 20 m on down, the currents are in phase.

These data, in conjunction with the model results, show the dynamical importance of the thin, fresh surface layer. Any surface forcing within the fjord acts on this thin surface layer, setting up a pressure gradient. The density contrast between this layer and the next is at times so large that mixing across the interface is negligible and the layers remain distinct. The pressure gradient in the top layer forces the next layer against the wind stress. Therefore, circulation models of the fjord with a fresh surface layer should include this thin layer in the dynamics.

d. Strait of Juan de Fuca

One final calculation considers the Strait of Juan de Fuca. The parameters (Table 2) for this case are quite different from those of a Norwegian fjord.

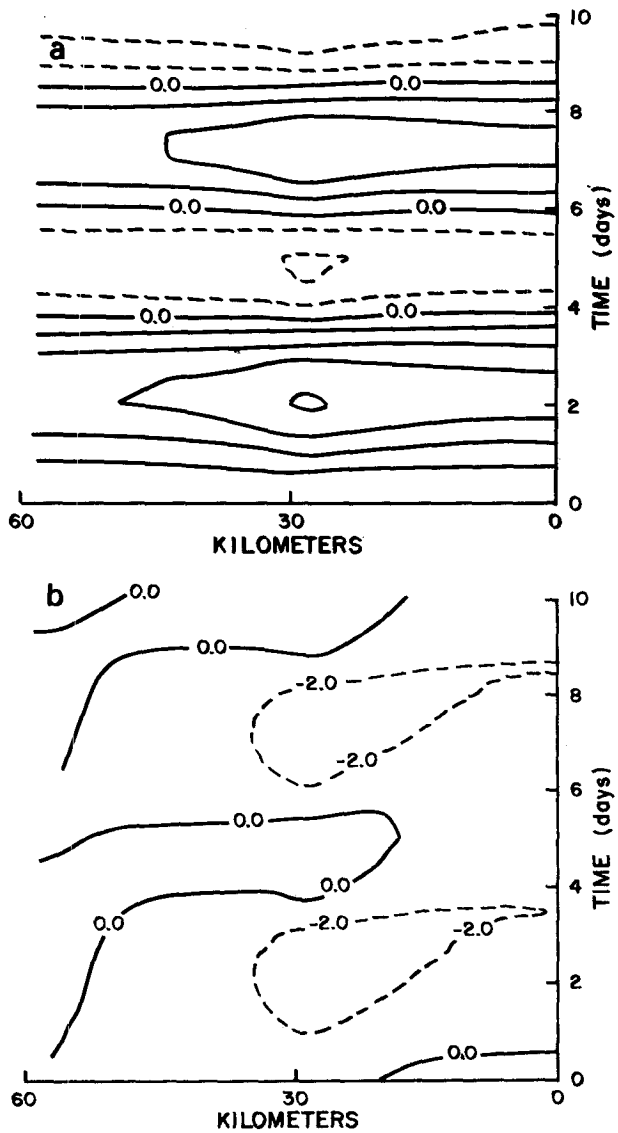

FIG. 10. Synoptic wind simulation. (a) Free surface and (b) pycnocline anomaly for a 5-day period sinusoidal wind stress. Physical parameters are the same as the basic case. Dashed lines indicate negative values. Contour intervals are (a) 2 cm, (b) 2 m.

The major difference is a change of aspect ratio. The wind forcing has the structure given by Fig. 3 and is northward over the eastern ocean.

The interface anomaly is presented in Fig. 12. Despite the change in geometry, the results are quite similar to the basic case. The major displacement of the interface occurs at the junction point, again controlled by the geostrophically balanced coastal currents. Note also that the majority of the fjord is only slightly affected by the disturbance at the coast, even after five days of steady forcing.

This result is compared to measurements in Juan de Fuca and offshore by Cannon *et al.* (1971) which shows an inclination of the internal density field of ~ 0.5 m km^{-1} after sustained southerly offshore winds. The model shows an internal inclination of 0.3 m km^{-1}.

No doubt, other dynamical processes are important in Juan de Fuca. The Coriolis acceleration is important because the Strait is not narrow compared to the internal deformation radius. Nevertheless, available data indicate that offshore rotational dynamics affect conditions in the strait.

5. Summary and conclusions

We have constructed a simple, linear transport model for a two-layer fjord connected with a two-layer ocean. The oceanic dynamics are rotational

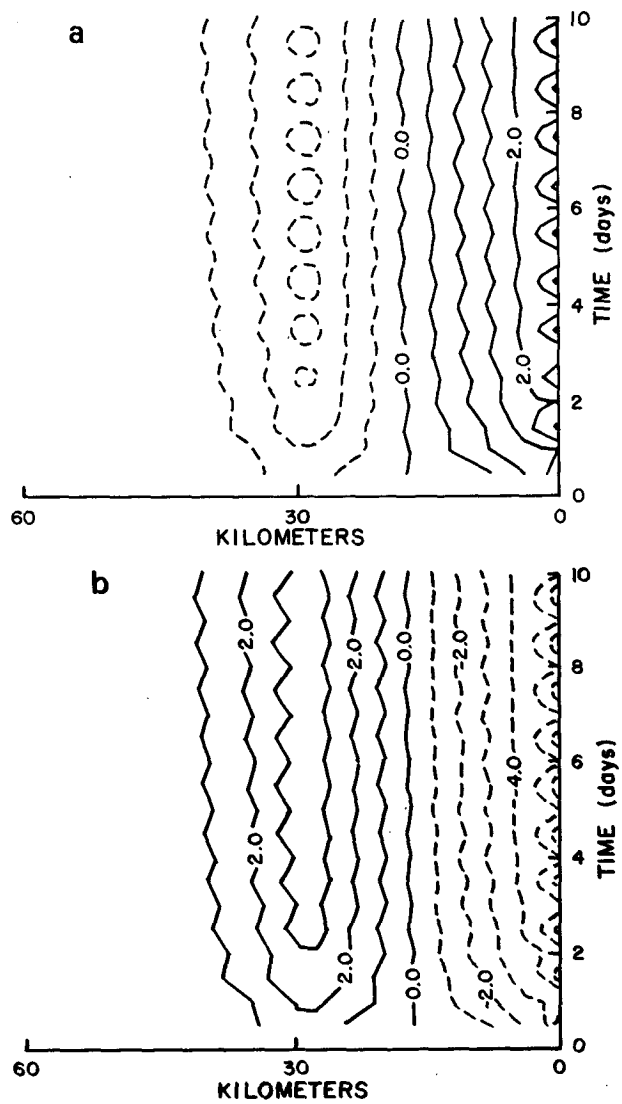

FIG. 11. Sea breeze simulation. (a) Free surface and (b) pycnocline anomaly. An up- and down-fjord wind (0.4 dyn cm^{-2}) is applied within 70 km of the fjord wall. Basic case parameters are used. Contour intervals are (a) 0.5 cm, (b) 1 m.

TABLE 2. Parameters for the Strait of Juan de Fuca simulation (parameters not given here are the same as Table 1).

$g' = 1$ cm s^{-2}
$H_1 = 30$ m
$H_2 = 120$ m
$L_f = 100$ km
$L_o = 900$ km

(β-plane) while the fjord is not affected by the Coriolis acceleration. This simple model neglects vertical mixing, nonlinear effects and geometric effects such as changes in the fjord width. Nevertheless, several interesting and previously unexpected features appear in the model simulations. They point out the need to reconsider some aspects of fjord circulation theory. These ideas can be tested by extending observational programs to include wind, currents and hydrography from nearby coastal areas.

The major conclusions of this research are the following.

1) Alongshore geostrophic coastal currents strongly control circulation in the fjord. This current has the effect of elevating (or depressing) the free surface and pycnocline, thereby controlling the displacement of these surfaces at the fjord mouth. The resulting pressure gradients within the fjord drive the circulation. Previous theories (Long, 1975; Pearson and Winter, 1978; Stigebrandt, 1980, 1981) use topographic conditions at the mouth to control fjord circulation. The interplay of these two control mechanisms will be considered with a nonlinear version of this model.

Field studies in Josenfjord, Norway (Svendsen, 1977; Svendsen and Thompson, 1978); Sandsfjord, Norway (Svendsen, 1980); Alberni Inlet, British Columbia (Stucchi and Bell, 1980) and the Strait of Juan de Fuca, Washington (Cannon *et al.*, 1971; Holbrook *et al.*, 1980) support our conclusions that wind-driven coastal currents influence fjord circulation. A study by Wang and Elliot (1978) shows a similar interaction between the Potomac River estuary and Chesapeake Bay.

2) The free-surface response to alongshore and across-shore wind stress is markedly different. Across-shore winds produce free surface slopes without changing the volume of water in the fjord. Alongshore winds, on the other hand, cause large changes in the volume of water in the fjord.

3) The surface tilt in the fjord is mainly a baroclinic effect. As the calculation in Section 3 shows, the surface basically mirrors the pycnocline.

4) Most simulations were made with and without sills. There was never any major effect from sills, due mainly to the linearity of the model. We expect a nonlinear model to respond more strongly to bottom topography.

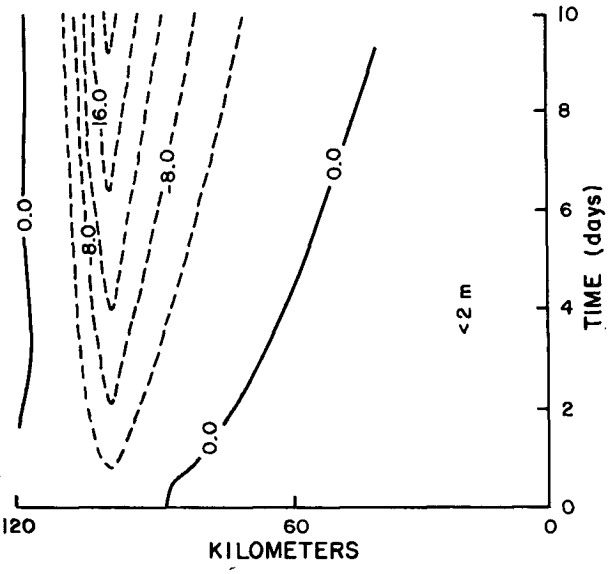

FIG. 12. Strait of Juan de Fuca simulation. X–t contour of the pycnocline anomaly. The impulsively started wind has the structure given in Fig. 3 and is northward on the eastern boundary. Physical parameters given in Table 2. Contour interval is 4 m.

5) The velocity change between the two layers in the fjord was as much as 10 cm s^{-1} for some cases. Similar shear is obtained from diffusively driven models (Officer, 1976, p. 116 ff) but they require diffusivities of 50 cm^2 s^{-1}, which is quite large, especially for fjords (Gade, 1970). These large velocity shears, due to coastal wind effects, will affect turbulence levels and diffusion within the fjord.

Future work with more complicated models and expanded field data sets will refine the various ideas presented here. However, we expect coastal dynamics to be an important factor in fjord circulation physics.

Acknowledgments. We wish to thank Martin Mork and Glenn Cannon for their discussions and critical analyses of the model. We also thank Eileen Hofmann for reading and commenting on the manuscript and Pat Heaton for her excellent work in typing various versions of the manuscript.

This work is supported by the Oceanography Section of the National Science Foundation, NSF Grant OCE-7925351. Partial support was provided by the Office of Naval Research Contract N00014-80-C-0076. Support for Harald Svendsen was provided by the National Science Foundation, NSF Grant OCE 7925351 and Statens Konsesjonsavgiftsfond (Norwegian governmental foundation).

APPENDIX

List of Symbols

A	horizontal eddy viscosity
$\alpha_1, \alpha_2, \lambda_1, \lambda_2$	constants used to uncouple the x transport equations
$\beta = \partial f/\partial y$	
$D(x)$	bottom topography variation from $z = 0$
$\Delta\rho$	density difference between the two layers.
f	Coriolis parameter
F_1, F_2	forcing function for uncoupled x transport equations
g	acceleration of gravity
$g' = \Delta\rho g/\rho$	reduced gravity
H_1, H_2	initial thickness of the two layers
h_1, h_2	variation of thickness from initial values
L_o, L_f	length of ocean and fjord, respectively
$\lambda = \sqrt{g'H}f^{-1}$	internal Rossby radius of deformation
$N^2 = \frac{-g}{\rho}\frac{\partial\rho}{\partial z}$	buoyancy frequency squared.
q_1, q_2	combinations of u_1, u_2 to uncouple x transport equation
τ^x, τ^y	surface wind stress in the east and north directions, respectively
u_1, u_2	x transport in each layer
v_1, v_2	y transport in each layer
x, y, z	Cartesian coordinates. Positive values are east, north and upward, respectively.

REFERENCES

Cannon, G. A., 1971: Statistical characteristics of velocity fluctuations at intermediate scales in a coastal plain estuary. *J. Geophys. Res.*, **76**, 5852–5858.

——, N. P. Laird and T. V. Ryan, 1971: Current Observations in Juan de Fuca Submarine Canyon. NOAA Tech. Rep. ERL 252-POL 14, 57 pp.

Devold, N., 1972: Den Norski Kyststrøm utenfor vestlandet (Hovedfagsppave i oseanografi). Thesis, University of Bergen, 57 pp.

Gade, H. G., 1970: Hydrographic Investigations in the Oslofjord, a study of water circulation and exchange processes. Rep. 24, Geophys. Inst., Div. A., University of Bergen, 3 Vols., 375 pp.

Helle, H., 1975: Oseanografiske Resipientundersøkelse av fjordene Rundt Bergen. Rep. Geophys. Inst., Div. A., University of Bergen, 72 pp.

——, 1978: Summer replacement of deep water in Byfjord, western Norway: Mass exchange across the sill induced by coastal upwelling. *Hydrodynamics of Estuaries and Fjords*, J. C. J. Nihoul, Ed., Elsevier, 441–464.

Herlinveaux, R. H., 1962: Oceanography of Saanich Inlet in Vancouver Island, British Columbia. *J. Fish Res. Board Can.*, **19**, 1–37.

Hermansen, H. O., 1974: Sognefjordens Hydrografi og Vannutveksling. Thesis, Geophys. Inst., University of Bergen, 56 pp.

Holbrook, J. R., R. D. Muench and G. A. Cannon, 1980: Seasonal observations of low frequency atmospheric forcing in the Strait of Juan de Fuca. *Fjord Oceanography*, H. J. Freeland, D. M. Farmer and C. D. Levings, Eds., NATO Conf.Ser., Ser. IV: Marine Sciences, Plenum, 305–318.

Hurlburt, H. E., and J. D. Thompson, 1973: Coastal upwelling on a β-plane. *J. Phys. Oceanogr.*, **3**, 16–32.

Issacson, E., and H. B. Keller, 1966: *Analysis of Numerical Methods*. Wiley, 541 pp.

Long, R. R., 1975: Circulations and density distribution in a deep strongly stratified, two-layer estuary. *J. Fluid Mech.*, **71**, 529–540.

O'Brien, J. J., and H. E. Hurlburt, 1972: A numerical model of coastal upwelling. *J. Phys. Oceanogr.*, **2**, 14–26.

Officer, C. B., 1976: *Physical Oceanography of Estuaries (and Associated Coastal Waters)*. Wiley, 465 pp.

Pearson, C. E., and D. F. Winter, 1978: Two-layer analysis of steady circulation in stratified fjords. *Hydrodynamics of Estuaries and Fjords*, J. C. J. Nihoul, Ed., Elsevier, 495–514.

Pedlosky, J., 1979: *Geophysical Fluid Dynamics*. Springer-Verlag, 624 pp.

Pickard, G. L., 1961: Oceanographic features of inlets in the British Columbia mainland coast. *J. Fish. Res. Board Can.*, **16**, 635–678.

Saelen, O. H., 1946: Temperature variations and heat transport in the Nordfjord. *Bergens Mus. Arbok*, 1946–47, Naturvitensk. Rekke, No. 6, 1–28.

Smith, R. L., 1968: Upwelling. *Oceanogr. Mar. Biol. Ann. Rev.*, **6**, 11–46.

Stigebrandt, A., 1980: A mechanism that regulates the mean longitudinal density gradient in the brackish layer in fjords with topographical control at their mouths. *Stratified Flows*, Proc. Second IAHR Symposium, Trondheim, 105–117.

——, 1981: A mechanism governing the estuarine circulation in deep, strongly stratified fjords. *Estuarine Coastal Mar. Sci.*, **13**, 197–211.

Stommel, H., and H. G. Farmer, 1952: Abrupt change in width in two-layer open flow. *J. Mar. Res.*, **11**, 205–214.

Stucchi, D. J., and W. H. Bell, 1980: Shelf-fjord exchange on the west coast of Vancouver Island. *Trans. Amer. Geophys. Union*, **61**, 280.

Svendsen, H., 1971: Investigation of the Norwegian coastal current off Egersund, September, 1968. *Arbok Univ. Bergen 1973*, Mat. Naturvitensk. Ser., No. 2, 19 pp.

——, 1977: A study of the circulation in a sill fjord on the west coast of Norway. *Mar. Sci. Commun.*, **3**, 151–209.

——, 1980: Exchange processes above sill level between fjord and coastal water. *Fjord Oceanography*, H. J. Freeland, D. M. Farmer and C. D. Levings, Eds., NATO Conf. Ser., Ser. IV: Marine Sciences, Plenum, 355–362.

——, and N. Utne, 1973: Hydrografi i Hardengerfjorden. Report for GACF (Government Advisory Council for Fjord Investigations).

——, and R. O. R. Y. Thompson, 1978: Wind-driven circulation in a fjord. *J. Phys. Oceanogr.*, **8**, 703–712.

Wang, D. P., and A. J. Elliot, 1978: Non-tidal variability in the Chesapeake Bay and Potomac River: Evidence for non-local forcing. *J. Phys. Oceanogr.*, **8**, 225–232.